RSC Advances

PAPER

View Article Online
View Journal | View Issue

Cite this: *RSC Adv.*, 2016, **6**, 53933

2,4-Diamino-5-(phenylthio)-5*H*-chromeno [2,3-*b*] pyridine-3-carbonitriles as green and effective corrosion inhibitors: gravimetric, electrochemical, surface morphology and theoretical studies

Chandrabhan Verma,[a] Lukman O. Olasunkanmi,[bc] I. B. Obot,[d] Eno E. Ebenso[b] and M. A. Quraishi*[a]

Received 24th February 2016
Accepted 25th May 2016

DOI: 10.1039/c6ra04900a

www.rsc.org/advances

The inhibition of mild steel corrosion in 1 M HCl by three newly synthesized 2,4-diamino-5-(phenylthio)-5*H*-chromeno[2,3-*b*]pyridine-3-carbonitriles (DHPCs) namely, 2,4-diamino-7-nitro-5-(phenylthio)-5*H*-chromeno[2,3-*b*]pyridine-3-carbonitrile (DHPC-1), 2,4-diamino-5-(phenylthio)-5H-chromeno[2,3-*b*] pyridine-3-carbonitrile (DHPC-2) and 2,4-diamino-7-hydroxy-5-(phenylthio)-5*H*-chromeno[2,3-*b*] pyridine-3-carbonitrile (DHPC-3) was studied using weight loss method, electrochemical techniques, surface morphology (SEM, AFM) studies and theoretical (quantum chemical calculations and molecular dynamic simulation) methods. The weight loss and electrochemical measurements showed that the inhibition efficiency increases with increasing inhibitor concentration and the relative trend of inhibition performance is DHPC-3 > DHPC-2 > DHPC-1. A potentiodynamic polarization study reveals that the investigated DHPCs act as mixed type inhibitors. The adsorption of the DHPCs on the mild steel surface obeys the Langmuir adsorption isotherm and involves both physisorption and chemisorption modes. The presence of the electron releasing –OH group at position seven on the chromenopyridine ring is considered to be responsible for the highest inhibition efficiency of DHPC-3 among the studied compounds. Whereas the presence of the electron withdrawing nitro ($-NO_2$) group at position seven on the chromenopyridine ring is responsible for the lowest inhibitive strength of DHPC-1. Quantum chemical calculations and molecular dynamic simulation studies were undertaken to provide mechanistic insight into the roles of the different substituents (–OH and $-NO_2$) on the corrosion inhibition behavior of the studied inhibitors.

1. Introduction

Iron and its alloys are widely used as construction materials in the petroleum, food, power production, chemical and electrochemical industries. This is due to their high thermal and mechanical stability, ease of fabrication and joining, and low cost.[1–3] However, these materials become gradually destroyed by corrosion upon exposure to the environment due to chemical or/and electrochemical reactions with the environment. Therefore, several efforts are being channeled towards preventing these undesirable reactions. Among the several available methods of corrosion protection, the utilization of synthetic corrosion inhibitors has become a popular method because of the ease and economic viability of the synthesis of these inhibitors, high inhibition efficiency, and practical-feasibility.[4–6] Most of the efficient corrosion inhibitors are organic compounds containing polar functional groups and π-electrons in form of triple or conjugated double bonds. These synthetic compounds inhibit corrosion by adsorbing on metallic surface. Generally, the adsorption of these inhibitors on the metal surfaces depends on numerous physicochemical properties such as nature of functional groups, steric factors, aromaticity, electron density at the donor atoms and p-orbital character of donating electrons and the electronic structure of the inhibitors molecules.[7] Previous literature had established that S-containing compounds show better inhibition efficiency in sulphuric acid solution, while N-containing compounds show better inhibition efficiency in hydrochloric acid solution.[8] Whereas, compounds containing both N- and S-atoms generally give rise to even better inhibition efficiency.[9,10]

[a]*Department of Chemistry, Indian Institute of Technology, Banaras Hindu University, Varanasi 221005, India. E-mail: maquraishi.apc@itbhu.ac.in; maquraishi@rediffmail.com; Fax: +91-542-2368428; Tel: +91-9307025126*

[b]*Department of Chemistry and Material Science Innovation & Modelling (MaSIM) Research Focus Area, Faculty of Agriculture, Science and Technology, North-West University (Mafikeng Campus), Private Bag X2046, Mmabatho 2735, South Africa*

[c]*Department of Chemistry, Faculty of Science, Obafemi Awolowo University, Ile-Ife, 220005, Nigeria*

[d]*Centre of Research Excellence in Corrosion, Research Institute, King Fahd University of Petroleum and Minerals, Dhahran 31261, Saudi Arabia*

The multicomponent reactions (MCRs) are of increasing importance in green organic and medicinal chemistry because they involve processes in which three or more components react directly to form a unique product, giving good atom economy.[11,12] Moreover, the MCRs are also valuable for green chemistry due to their operational simplicity, small number of steps, facile automation, minimum waste generation (as a result of reduced number of work-ups), simple purification procedure, which enhances synthetic efficiency, resources and time saving.[13–15]

In view of this, we report on the corrosion inhibition efficiency of three chromenopyridines namely, 2,4-diamino-7-nitro-5-(phenylthio)-5*H*-chromeno[2,3-*b*]pyridine-3-carbonitrile (DHPC-1), 2,4-diamino-5-(phenylthio)-5*H*-chromeno[2,3-*b*]pyridine-3-carbonitrile (DHPC-2) and 2,4-diamino-7-hydroxy-5-(phenylthio)-5*H*-chromeno[2,3-*b*]pyridine-3-carbonitrile (DHPC-3) for mild steel in 1 M HCl. The investigated chromenopyridines were synthesized by MCRs. The study was performed using weight loss, potentiodynamic polarization, electrochemical impedance spectroscopy (EIS), scanning electron microscopy (SEM), atomic force microscopy (AFM), quantum chemical and molecular dynamics calculations methods. The choice of these compounds as corrosion inhibitors is based on the consideration that they can be easily synthesized *via* green method using readily available chemicals in one step, in addition to their high solubility in the test solution, which enhances their inhibition efficiency. Furthermore, literature survey reveals that the inhibitive property of the studied chromenopyridines has not been reported earlier, which portrays the compounds to be novel potential corrosion inhibitors.

2. Experimental section

2.1. Materials

2.1.1. Electrode and reagents. The mild steel specimens for weight loss, electrochemical measurements and surface morphology studies were cut form commercially available mild steel sheet having chemical composition (wt%): C (0.076), Mn (0.192), P (0.012), Si (0.026), Cr (0.050), Al (0.023), and Fe (balance). The exposed surface of the working electrodes were cleaned successively with emery papers of different grades (600, 800, 1000, and 1200), washed with deionized water, degreased with acetone, ultrasonically cleaned with ethanol and stored in moisture free desiccator before used in the experiments. Hydrochloric acid (37% HCl from MERCK) and double distilled water were used for the preparation of 1 M HCl test solution.

2.1.2. Inhibitors synthesis. The chromenopyridines used in the present study were synthesized by one step MCRs as previously described[16] and the synthetic route is shown in Fig. 1. The progress of reaction was checked by using thin layer chromatographic (TLC) method. After completion of reaction, the products were dissolved in DMF and undissolved components were removed through filtration. Addition of water to DMF results in the crystallization of pure product. The characterization data of the synthesized compounds are given in Table 1.

2.2. Methods

2.2.1. Weight loss measurements. Cleaned, dried and accurately weighted mild steel specimens having dimension 2.5 × 2.0 × 0.25 cm^3 were immersed in 1 M HCl without and with different concentrations of DHPCs for 3 h. The specimens were then removed, washed with distilled water and acetone, dried in moisture free desiccator, and again weighed accurately. To ensure the reproducibility of the weight loss results, each experiment was triply performed and average values were recorded at each concentration of the inhibitors. From the observed average weight loss, the inhibition efficiency (η%) was calculated as:[17]

$$\eta\% = \frac{w_o - w_i}{w_o} \times 100 \quad (1)$$

where w_0 and w_i are the weight loss values in the absence and presence of DHPCs at different concentrations, respectively.

2.2.2. Electrochemical measurements. The mild steel specimens with exposed area of 1 cm^2 (one sided) were utilized for all electrochemical measurements. The experiments were performed under potentiodynamic condition using Gamry Potentiostat/Galvanostat (Model G-300) instrument. Gamry Echem Analyst 5.0 software was used for fitting, simulation and analysis of all electrochemical data. The instrument consist of mild steel working electrode (WE), platinum as counter electrode and a saturated calomel electrode (SCE) as reference electrode. Before starting the electrochemical experiments, the working electrode was allowed to corrode freely for sufficient time in order to attain steady open circuit potential (OCP). During the polarization measurements, the cathodic and anodic Tafel slopes were recorded by changing the electrode potentials from −0.25 to +0.25 V *vs.* corrosion potential (E_{corr}) at a constant sweep rate of 1.0 mV s^{-1}. The corrosion current density (i_{corr}) was calculated by extrapolating the linear segments of the Tafel plots (cathodic and anodic). From the

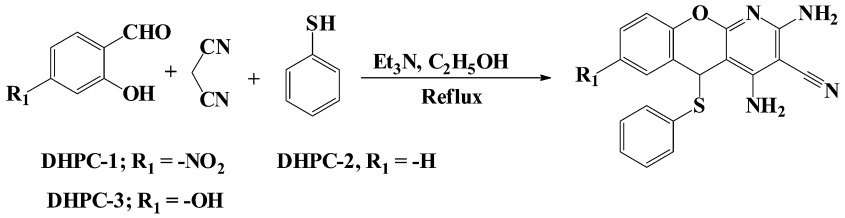

Fig. 1 Synthetic route of the studied DHPCs.

calculated i_{corr} values, the inhibition efficiency was calculated using the relation:[17]

$$\eta\% = \frac{i^0_{corr} - i^i_{corr}}{i^0_{corr}} \times 100 \quad (2)$$

where, i^0_{corr} and i^i_{corr} are corrosion current densities in the absence and presence of DHPCs, respectively.

Electrochemical impedance measurements were carried out at the OCP in the frequency range of 100 kHz to 0.01 Hz using AC signal of amplitude 10 mV peak to peak. The charge transfer resistances were calculated from the Nyquist plots. The inhibition efficiency was calculated using the equation:[17]

$$\eta\% = \frac{R^i_{ct} - R^0_{ct}}{R^i_{ct}} \times 100 \quad (3)$$

where, R^0_{ct} and R^i_{ct} are charge transfer resistances in the absence and presence of DHPCs, respectively.

2.2.3. SEM, EDX and AFM measurements. For surface analysis, the cleaned mild steel specimens of were allowed to corrode for 3 h in the absence and presence of optimum concentration of DHPCs. Thereafter, the specimens retrieved, washed with water, dried and employed for SEM, EDX and AFM analysis. The SEM model Ziess Evo 50 XVP was used to investigate the micromorphology of mild steel surface at 500× magnification. Chemical compositions of the inhibited and uninhibited specimens were recorded by an EDX detector coupled to the SEM. NT-MDT multimode AFM, Russia, 111 controlled by solvers canning probe microscope controller was employed for AFM surface analysis. The single beam cantilever having resonance frequency in the range of 240–255 kHz in semi contact mode with corresponding spring constant of 11.5 N m^{-1} with NOVA programme was used for image interpretation. The scanning area during AFM analysis was 5 mm × 5 mm.

2.2.4. Molecular dynamics simulations. Forcite module in the Material Studio Software 7.0 from BIOVIA-Accelrys, USA was adopted to carry out the quench molecular dynamic (MD) simulations. The simulation was carried out with Fe (110) crystal with a slab thickness of 5 Å. The Fe (110) plane was enlarged to a (8 × 8) supercell to provide a large surface for the interaction with the inhibitors. After that, a vacuum slab with 30 Å thickness was built above the Fe (110) plane. For the whole simulation procedure, the Condensed-phase Optimized Molecular Potentials for Atomistic Simulation Studies (COMPASS) force field was used to optimize the structures of all components of the system of interest. The MD simulations were performed in NVT canonical ensemble at 298 K with a time step of 0.1 fs and a total simulation time of 100 ps using Anderson thermostat.

Table 1 IUPAC name, molecular structure, molecular formula, melting point and analytical data of the studied DHPCs

S.No.	IUPAC name and abbreviation of inhibitor	Chemical structure	Molecular formula and M.P. and analytical data
1	2,4-Diamino-7-nitro-5-(phenylthio)-5*H*-chromeno [2,3-*b*]pyridine-3-carbonitrile (DHPC-1)	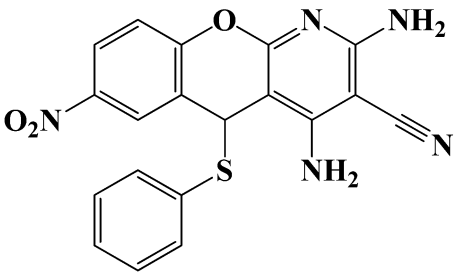	$C_{19}H_{13}N_5O_3S$ (mol wt 391.07); yield: 78%, mp; 206–208 °C; FT-IR (KBr, cm^{-1}): 3558, 3438, 3324, 2961, 2863, 2256, 1668, 1551, 1446, 1253, 1184, 1036, 962, 862, 774, 672, 632; ^{1}H NMR (300 MHz, DMSO) δ (ppm): 5.136, 6.387, 7.129–7.238, 7.215–7.393, 7.396–7.468, 7.834, 7.935–8.073
2	2,4-Diamino-5-(phenylthio)-5*H*-chromeno [2,3-*b*] pyridine-3-carbonitrile (DHPC-2)	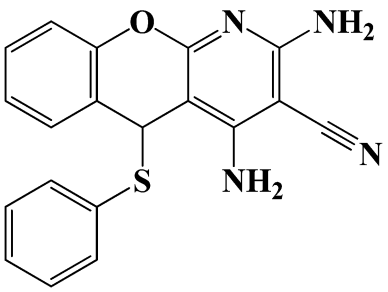	$C_{19}H_{14}N_4OS$, (mol wt 346.08), yield: 84%, mp; 214–216 °C; FT-IR (KBr, cm^{-1}): 3571, 3426, 3312, 2947, 2852, 2238, 1573, 1456, 1262, 1179, 1022, 935, 892, 729, 635; ^{1}H NMR (300 MHz, DMSO) δ (ppm): 5.117, 6.218, 6.83–6.936, 6.964–7.982, 7.126–7.238, 7.329–7.398, 7.846
3	2,4-Diamino-7-hydroxy-5-(phenylthio)-5*H*-chromeno [2,3-*b*]pyridine-3-carbonitrile (DHPC-3)	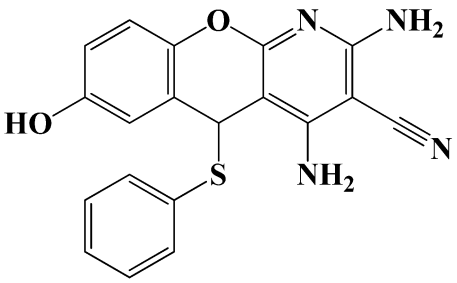	$C_{19}H_{14}N_4O_2S$, (mol wt 261.09), $C_{19}H_{14}N_4O_2S$, (mol wt 362.40), yield: 68–70%, mp; 256–258 °C; FT-IR (KBr, cm^{-1}): 3658, 3554, 3368, 2942, 2876, 2264, 1556, 1433, 1228, 1152, 1045, 949, 873, 746, 578: ^{1}H NMR (300 MHz, DMSO) δ (ppm): 5.124, 6.135, 6.693–6.789, 6.792–6.836, 7.264, 7.348–7.394, 7.862

Table 2 The weight loss parameters obtained for mild steel in 1 M HCl containing different concentrations of DHPCs

Inhibitor	Conc (mol L^{-1})	C_R (mg cm^{-2} h^{-1})	Inhibition efficiency (η%)	Surface coverage (θ)
Blank	0.0	7.66	—	—
DHPC-1	2.55×10^{-5}	2.86	62.66	0.6266
	5.11×10^{-5}	1.20	84.33	0.8433
	7.67×10^{-5}	0.73	90.46	0.9046
	10.22×10^{-5}	0.53	93.08	0.9308
	12.70×10^{-5}	0.36	95.30	0.9530
DHPC-2	2.55×10^{-5}	2.46	67.88	0.6788
	5.11×10^{-5}	1.03	86.55	0.8655
	7.67×10^{-5}	0.60	92.16	0.9216
	10.22×10^{-5}	0.40	94.77	0.9477
	12.70×10^{-5}	0.26	96.60	0.9660
DHPC-3	2.55×10^{-5}	2.10	72.58	0.7258
	5.11×10^{-5}	0.86	88.77	0.8877
	7.67×10^{-5}	0.46	93.99	0.9399
	10.22×10^{-5}	0.33	95.69	0.9569
	12.70×10^{-5}	0.16	97.91	0.9791

Table 3 Variation of C_R and η% with temperature in the absence and presence of optimum concentration of DHPCs in 1 M HCl

	Corrosion rate (C_R) (mg cm^{-2} h^{-1}) and inhibition efficiency (η%)							
	Blank		DHPC-1		DHPC-2		DHPC-3	
Temperature (K)	C_R	η%	C_R	η%	C_R	η%	C_R	η%
308	7.66	—	0.36	95.30	0.26	96.60	0.16	97.91
318	11.0	—	0.96	91.27	0.76	93.09	0.46	95.81
328	14.3	—	2.10	85.31	1.73	87.90	1.20	91.60
338	18.6	—	4.23	77.25	3.80	79.56	3.23	82.63

2.2.5. Quantum chemical calculations. The quantum chemical studies in the present work were carried out by using similar computational approach employed in some previous studies.[18,19] Quantum chemical calculations were carried out on the studied compounds in order to provide corroborative explanations for the inhibition activities of the DHPCs at molecular level. The optimized structures and electronic energy parameters were obtained by using the B3LYP/6-31G(d) model[20–22] of the density functional theory (DFT) method. The optimized structures were confirmed to correspond to true energy minima by the absence of an imaginary frequency in the force constant calculations. All the quantum chemical parameters used in providing theoretical explanations for the corrosion inhibition properties of the studied compounds are those of the most stable ground state geometries. Quantum chemical calculations were carried out with the aid of Gaussian 09 suite software.[23] The energy of the highest occupied molecular orbital (E_{HOMO}), the energy of the lowest unoccupied molecular orbital (E_{LUMO}), the energy band gap ($\Delta E = E_{LUMO} - E_{HOMO}$), and the dipole moment of the optimized structures were obtained and recorded. The absolute electronegativity (χ) of the inhibitor molecule was calculated using the equations:[19,20]

$$\chi = \frac{1}{2}(E_{HOMO} + E_{LUMO}) \quad (4)$$

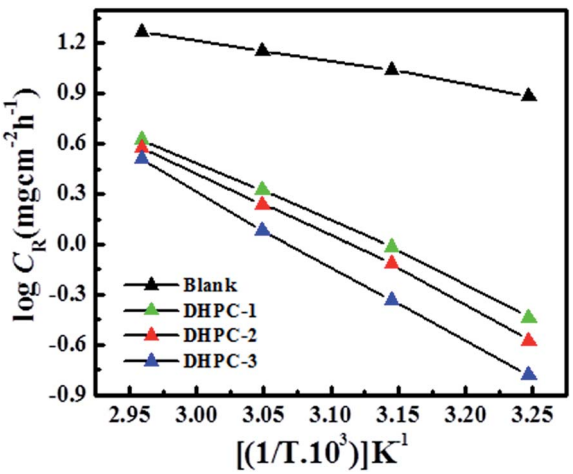

Fig. 2 Arrhenius plots for the corrosion of mild steel in 1 M HCl in the presence of the studied inhibitors.

The fraction of electrons transferred from the inhibitor molecule to the metal, (ΔN) was calculated according to the equation:[19,24]

$$\Delta N = \frac{\chi_{Fe} - \chi_{inh}}{2(\eta_{Fe} + \eta_{inh})} \quad (5)$$

where χ_{Fe} and χ_{inh} are the electronegativity values of Fe and inhibitor respectively, while η_{Fe} and η_{inh} denote the hardness values of Fe and inhibitor respectively. Pearson's

Table 4 Activation energies for mild steel dissolution in 1 M HCl in the absence and presence of optimum concentration of DHPCs

Inhibitor	E_a (kJ mol^{-1})
Blank	28.48
DHPC-1	69.89
DHPC-2	76.54
DHPC-3	84.38

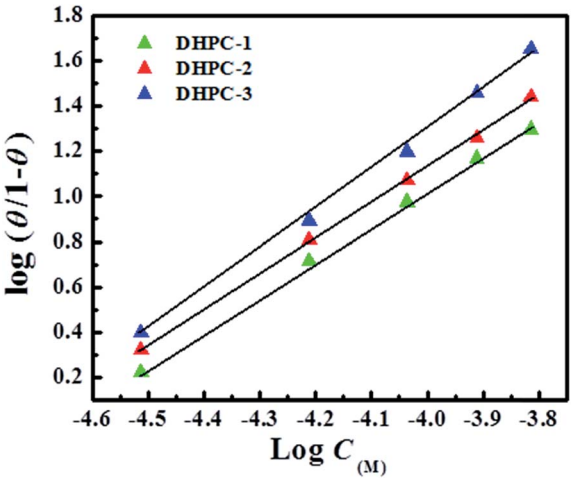

Fig. 3 Langmuir adsorption isotherms for mild steel in 1 M HCl in the presence of the studied DHPCs at different concentration.

Table 5 The values of K_{ads} and ΔG°_{ads} for mild steel in 1 M HCl in the absence and presence of optimum concentration of DHPCs at different temperatures

	K_{ads} (10^4 M^{-1})				$-\Delta G^{\circ}_{ads}$ (kJ mol^{-1})			
Inhibitor	308	318	328	338	308	318	328	338
DHPC-1	2.38	1.24	0.69	0.40	36.10	35.56	35.10	34.66
DHPC-2	3.32	1.60	0.87	0.46	36.96	36.22	35.70	35.05
DHPC-3	5.38	2.70	1.31	0.57	38.19	37.61	36.82	35.61

electronegativity scale[6] assigns a 7 eV mol^{-1} for χ_{Fe}, while η_{Fe} is approximately equal to 0 eV mol^{-1} for bulk Fe.

Fukui functions are often utilized to predict the atomic sites that are susceptible to nucleophilic and electrophilic attacks in an inhibitor molecule. The sites for nucleophilic and electrophilic attacks are informed by the Fukui indices f^+ and f^- respectively. Yang and Mortier[25] proposed the use of Mulliken population analysis (MPA) and finite difference (FD) approximations for the calculation of Fukui functions, and the corresponding equations for f^+ and f^- respectively are:[18,19,25]

$$f_k^+ = \rho_{k(N+1)}(r) - \rho_{k(N)}(r) \quad (6)$$

$$f_k^- = \rho_{k(N)}(r) - \rho_{k(N-1)}(r) \quad (7)$$

where $\rho_{k(N+1)}$, $\rho_{k(N)}$ and $\rho_{k(N-1)}$ are the electron densities of the molecular species with $N+1$ electrons, N electrons and $N-1$ electrons respectively. The numerical values of $f^+$and f^- were plotted as graphical electron density isosurfaces with the aid of Multiwfn software.[26,27]

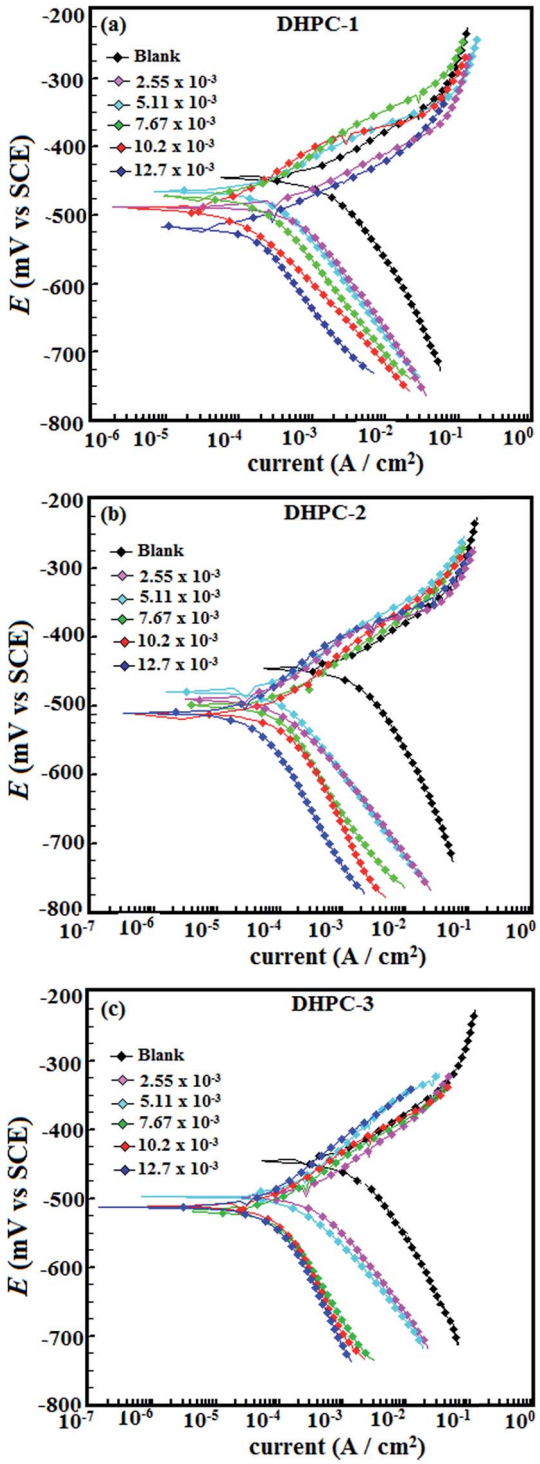

Fig. 4 Polarization curves recorded for mild steel in the absence and presence of different concentrations DHPC-1 (a), DHPC-2 (b), and DHPC-3 (c).

3. Results and discussions

3.1. Weight loss experiments

3.1.1. Effect of inhibitors concentration. The weight loss experiments were carried out for 3 h immersion time at 308 K in the absence and presence of different concentrations of the studied compounds. The calculated weight loss parameters such as corrosion rate (C_R), surface coverage (θ) and corresponding inhibition efficiencies (η%) are given in Table 2. From the results shown in Table 2 it can be seen that the inhibition efficiency of the three compounds increases with increasing concentration. The maximum inhibition efficiency was obtained at 12.70 × 10^{-5} mol L^{-1} concentration. Further increase

in DHPCs concentration did not cause any significant change in the inhibition performance. The relative strengths of inhibition the studied compounds follow the order DHPC-3 > DHPC-2 > DHPC-1. The highest inhibition efficiency of the DHPC-3 among the studied inhibitors is attributed to the presence of the electron donating –OH group at position seven of the chromenopyridine ring. In contrast, the lowest inhibition efficiency of the DHPC-1 could be as a result of electron withdrawing nature of the $-NO_2$ group substituted at position seven of the chromenopyridine ring.[28]

3.1.2. Effect of temperature. In order to study the influence of temperature on the corrosion inhibition efficiency of the investigated inhibitors, the weight loss experiments were carried out at different temperatures (308–338 K) in the absence and presence of optimum concentration of the DHPCs. It is observed from the results depicted in Table 3 that the corrosion rate increases and inhibition efficiency decreases with increasing inhibitors concentration. The increased corrosion rate at elevated temperature could be as a result of increased average molecular speed of the inhibitor molecules that weakens the adsorption tendency of the inhibitors on the metallic surface.[29] The temperature dependency of the corrosion rate can be represented by the Arrhenius equation:[30]

$$\log(C_R) = \frac{-E_a}{2.303RT} + \log A \quad (8)$$

where C_R is the corrosion rate in mg cm^{-2} h^{-1}, A is the Arrhenius pre-exponential factor, R is the gas constant and T is the absolute temperature. The Arrhenius plots shown in Fig. 2 give a straight line between log C_R *versus* $1/T$ from the slopes ($-\Delta E_a/2.303R$) of which values of activation energies were calculated for all the inhibitors and the results are listed in Table 4. It is observed from the results in Table 4 that in presence of DHPCs, E_a attains the cooperatively higher values of 69.89 kJ mol^{-1} for DHPC-1, 76.54 kJ mol^{-1} for DHPC-2, and 84.38 kJ mol^{-1} for DHPC-3 as compared to in their absence ($E_a = 28.48$ kJ mol^{-1}). It was further observed that the order of E_a was consisted with order of inhibition efficiency *i.e.* a higher value of E_a was observed for a more efficient inhibitor. The increased values of E_a in the presence of DHPCs suggested that higher energy barrier has been established for the corrosion reactions due to the adsorption of the inhibitors on the metallic surface.[31]

3.1.3. Adsorption isotherm. The adsorption of inhibitors at metal/electrolyte interface is a very important topic in corrosion inhibition study because it provides some insights into the inhibition mechanism. The adsorption of an organic adsorbate at metal/electrolyte interface depends upon the nature of the testing media, the chemical structure of the inhibitor, the charge distribution of the inhibitor, nature and surface charge of the metal. In the present study, the calculated surface coverage at different concentrations of the investigated inhibitors was subjected to different adsorption isotherm models in order to find best adsorption isotherm. However, the Langmuir adsorption isotherm gives the best fit having values of regression coefficient (R^2) very close to unity. The Langmuir isotherm can be represented by the equation:[32]

$$K_{ads}C = \frac{\theta}{1-\theta} \quad (9)$$

where K_{ads} is the equilibrium constant of the adsorption process, C is the inhibitors concentration and θ is the surface coverage, which was derived from the weight loss experiments. The Langmuir isotherm (Fig. 3) gives straight lines for the plots of $\log \theta/1 - \theta$ *versus* $\log C$ from which values of K_{ads} were calculated for the studied inhibitors. The K_{ads} is related to the Gibbs' free energy of adsorption according to the equation:

$$\Delta G^{\circ}_{ads} = -RT \ln(55.5K_{ads}) \quad (10)$$

where T is the absolute temperature and R is the universal gas constant. The numerical value of 55.5 represents the molar concentration of water in acid solution. The calculated values of K_{ads} and ΔG°_{ads} are given in Table 5. Generally, the value of K_{ads} represents the affinity of inhibitor for adsorption on the metallic surface and a high value of K_{ads} is consistent with high

Table 6 Tafel polarization parameters for mild steel in 1 M HCl solution in the absence and presence of different concentrations of DHPCs

Inhibitor	Conc mol L^{-1}	E_{corr} (mV per SCE)	β_a (μA cm^{-2})	β_c (mV dec^{-1})	i_{corr} (mV dec^{-1})	η%	θ
Blank	—	−445	70.5	114.6	1150	—	—
DHPC-1	2.55×10^{-5}	−487	62.0	129.5	438.6	61.68	0.6186
	5.11×10^{-5}	−472	74.5	110.3	156.0	86.43	0.8643
	7.67×10^{-5}	−474	57.9	105.5	114.3	90.06	0.9006
	10.2×10^{-5}	−491	74.4	84.6	67.6	94.12	0.9412
	12.7×10^{-5}	−517	65.4	60.4	46.8	95.93	0.9593
DHPC-2	2.55×10^{-5}	−507	68.7	144.4	384.0	66.60	0.6660
	5.11×10^{-5}	−496	76.6	129.7	154.3	86.58	0.8658
	7.67×10^{-5}	−509	69.5	122.7	94.2	91.80	0.9180
	10.2×10^{-5}	−515	110.0	120.6	42.6	96.29	0.9629
	12.7×10^{-5}	−513	69.5	162.3	28.4	97.53	0.9753
DHPC-3	2.55×10^{-5}	−497	74.0	106.6	286.3	75.10	0.7510
	5.11×10^{-5}	−496	91.6	88.7	144.0	87.47	0.8747
	7.67×10^{-5}	−517	74.7	156.4	78.4	93.18	0.9318
	10.2×10^{-5}	−511	72.4	142.7	34.6	96.99	0.9699
	12.7×10^{-5}	−512	88.5	143.7	22.6	98.03	0.9803

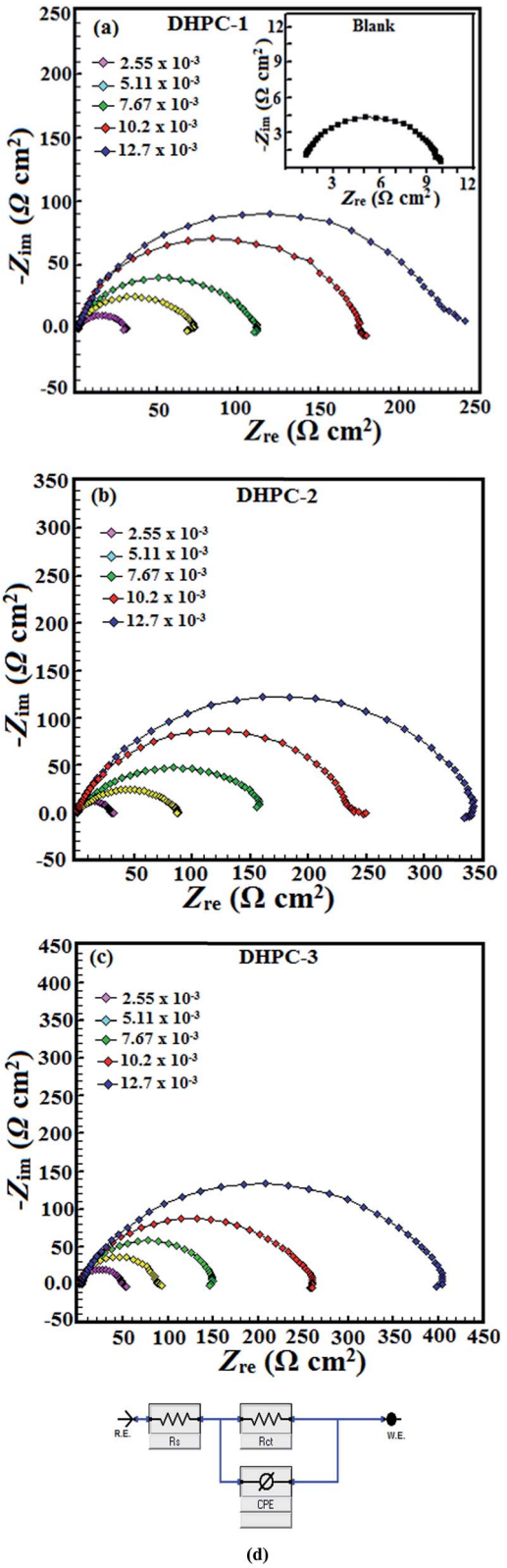

Fig. 5 (a–c): Nyquist plots recorded for mild steel in 1 M HCl in the absence and presence of different concentrations of (a) DHPC-1, (b) DHPC-2, and (c) DHPC-3 (d) equivalent circuit used for fitting and analyzing the electrochemical data.

adsorption ability. In the present study the values of K_{ads} for the studied inhibitors follow the order DHPC-3 > DHPC-2 > DHPC-1, which is in accordance with the order of inhibition efficiency. The large negative values of ΔG°_{ads} for the studied inhibitors indicate that these compounds possessed strong tendency to adsorb spontaneously on the mild steel surface.[33,34] Literature survey reveals that the values of ΔG°_{ads} in between -20 kJ mol^{-1} to -40 kJ mol^{-1} are consistent with physiochemisorption. In our present case, the values of ΔG°_{ads} varies from -34.66 kJ mol^{-1} to 38.19 kJ mol^{-1} suggesting that the adsorption of the investigated inhibitors on mild steel surface involves electrostatic interaction between charged inhibitors and charged mild steel surface (physisorption) as well as charge sharing or transfer from the inhibitor molecules to the metal surface to form a coordinate type of bond (chemisorption).[35,36]

3.2. Electrochemical measurements

3.2.1. Potentiodynamic polarization study. The potentiodynamic polarization study was carried out in the absence and presence of different concentrations of the investigated inhibitors to gather information about kinetics of the anodic and cathodic half reactions. The polarization curves for mild steel dissolution in 1 M HCl with and without inhibitors are shown in Fig. 4. The values of potentiodynamic polarization parameters namely, corrosion potential (E_{corr}), corrosion current density (i_{corr}), anodic and cathodic Tafel slopes (β_a, β_c) were obtained by extrapolation of the linear segments of the anodic and cathodic Tafel curves. The polarization parameters along with the calculated inhibition efficiency at various concentrations of all the studied inhibitors are given in Table 6. From the results in Fig. 4 and Table 6, it is observed that all the three inhibitors considerably reduced the corrosion current densities for both anodic and cathodic half-reactions, suggesting that both anodic dissolution of mild steel and cathodic reduction of hydrogen ions were inhibited. Obviously, greater decrease in the values of i_{corr} was observed at high inhibitors concentration. In general, an inhibitor can be classified as anodic or cathodic type, if the shift in the E_{corr} is higher than 85 mV with respect to E_{corr} of the blank, and as a mixed type inhibitor, if shift in E_{corr} is lower 85 mV.[37,38] In our present investigation maximum displacement in the E_{corr} values were 72 mV for DHPC-1, 70 mV for DHPC-2 and 72 mV for DHPC-3. It can also be observed from the results in Table 6 that the change in the values of β_c are more prominent as compared to that of β_a, suggesting that the studied compounds mixed type inhibitors with predominantly cathodic inhibitive effects.

3.2.2. Electrochemical impedance spectroscopy (EIS). The EIS is a widely used technique to understanding the mechanism of corrosion, passivation and charge transfer at the metal/electrolyte interface. The Nyquist curves for mild steel corrosion in 1 M HCl without and with various concentrations of the studied inhibitors obtained after 30 min immersion time are given Fig. 5a–c. It is noticeable that the shapes of Nyquist plots are similar for all the systems, which suggest that presence of inhibitors did not cause any significant change in the corrosion mechanism. In the present study, the Nyquist plots give

Table 7 EIS parameters obtained for mild steel in 1 M HCl in the absence and presence of different concentrations of DHPCs

Inhibitor	Conc mol L^{-1}	R_s (Ω cm^2)	R_{ct} (Ω cm^2)	n	C_{dl} (μF cm^{-2})	η%	θ
Blank	—	1.12	9.58	0.827	106.21	—	—
DHPC-1	2.55×10^{-5}	0.917	26.28	0.839	67.25	63.54	0.6354
	5.11×10^{-5}	0.925	69.77	0.815	59.92	86.26	0.8626
	7.67×10^{-5}	1.124	107.56	0.847	45.50	91.09	0.9109
	10.2×10^{-5}	0.784	175.2	0.892	44.86	94.53	0.9453
	12.7×10^{-5}	0.956	245.4	0.845	43.42	96.09	0.9609
DHPC-2	2.55×10^{-5}	0.811	30.62	0.835	59.36	69.53	0.6953
	5.11×10^{-5}	1.047	85.38	0.863	52.42	88.77	0.8877
	7.67×10^{-5}	1.115	148.4	0.837	39.61	93.54	0.9354
	10.2×10^{-5}	0.804	241.7	0.808	33.27	96.03	0.9603
	12.7×10^{-5}	0.844	338.0	0.812	28.56	97.16	0.9716
DHPC-3	2.55×10^{-5}	1.047	39.50	0.890	54.47	75.74	0.7574
	5.11×10^{-5}	1.019	88.79	0.886	45.63	89.21	0.8921
	7.67×10^{-5}	0.802	152.9	0.825	32.84	93.73	0.9373
	10.2×10^{-5}	0.948	253.9	0.810	27.87	96.22	0.9622
	12.7×10^{-5}	1.186	390.4	0.890	23.11	97.54	0.9754

imperfect capacitive semicircle, which is often associated with different phenomena such as roughness and other forms of inhomogeneities of the metal surface, distribution of the surface active sites, grain boundaries and presence of impurities.[39] The electrical equivalent circuit used to analyze the Nyquist plots is shown in Fig. 5b. The electrical equivalent circuit consists of the solution resistance (R_s), the charge transfer resistance (R_{ct}) and a constant phase element (CPE). In the present case, a CPE was used rather than pure double layer capacitance (C_{dl}) in order to take into account the mild steel surface roughness and heterogeneities, impurities, formation of porous layer, dislocation, adsorption of inhibitors, and grain boundaries. The impedance of the CPE (ZCPE) can be represented as:[40,41]

$$Z_{CPE} = \left(\frac{1}{Y_0}\right)\left[(j\omega)_n\right]^{-1} \quad (11)$$

where Y_0 is the CPE constant, ω is the angular frequency, j is the imaginary number, and n is the phase shift (exponent), which provides a measure of surface inhomogeneity resulted due to inhibitors adsorption, porous film formation, surface roughness *etc.* On the basis of the value of n, CPE can represent resistance ($n = 0$), capacitance ($n = 1$), inductance ($n = 1$) or Warburg impedance ($n = 0.5$). The value of C_{dl} with and without inhibitors was calculated using the equation:[42]

$$C_{dl} = Y_0(\omega_{max})^{n-1}$$

where ω_{max} is the frequency at which the imaginary part of impedance has attained the maximum (rad s^{-1}) value. The calculated EIS parameters such as R_s, R_{ct}, n, C_{dl}, η% and surface coverage (θ) are reported in Table 7. The results in Table 7 show that the values of R_{ct} increase with increase in inhibitors concentration. The increased value of R_{ct} in the presence of inhibitors is as a result of the formation of protective adsorption layer on the steel surface, which isolates the metal from the aggressive acid solution.[43,44] The decreased value of C_{dl} in the presence of the investigated inhibitors suggests a decrease in the dielectric constant and an increase in the thickness of the electrical double layer. Moreover, it is further observed that the increase in the values of R_{ct} and decrease in the values of C_{dl} is more pronounced at higher inhibitors concentration.[43,44]

The Bode phase and impedance plots for mild steel in the absence and presence of different concentrations of the studied compounds are shown Fig. 6a–c. Careful inspection of the Bode plots showed that the values of phase angle increase in the presence of inhibitors as compared to that of the blank acid solution. The relatively high values of phase angles in presence of the inhibitors is attributed to increased surface smoothness of the mild steel specimens, which may be due to adsorption of the inhibitors on the steel surface.[45,46] However, the ideal capacitive behavior of electric double layer was not observed in the present study, as the value of phase angle and slope could not achieved at 90° and −1, respectively.[45,46] The deviation from ideal capacitive behavior in this study is due to surface inhomogeneities of structural and interfacial origin.

3.3. Surface measurements

3.3.1. Scanning electron microscopy (SEM). In order to further study the influence of the studied inhibitors on the corrosion of mild steel in acid solution, the SEM micrographs of abraded mild steel surface, and mild steel surfaces in 1 M HCl solution in the absence and presence of optimum concentration of the studied DHPCs were recorded after 3 h immersion time. Fig. 7a depicts the SEM micrograph of abraded mild steel surface which shows only the abrading scratches and lining pits. The SEM image of the mild steel specimen retrieved from blank acid solution (Fig. 7b) showed highly corroded and damaged surface revealing a mountain-like appearance, which is due to free acid corrosion of mild steel in the absence of the inhibitors. However, in the presence of the inhibitors, the surface morphology of the mild steel specimens (Fig. 7c–e) are remarkably improved, which may be as a result of the formation of protective film of the inhibitor molecules on the steel surface.

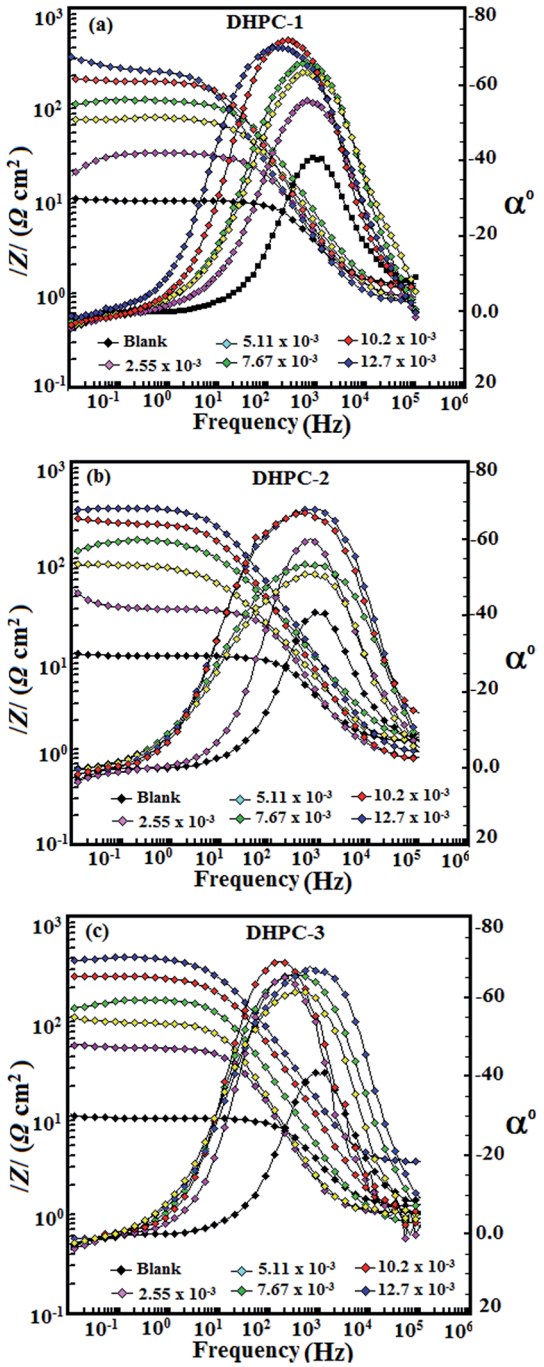

Fig. 6 Bode impedance modulus (log f *vs.* log|Z|) and phase angle (log f *vs.* α^0) plots for mild steel in 1 M HCl in the absence and presence of different of different concentrations of (a) DHPC-1, (b) DHPC-2, and (c) DHPC-3.

3.3.2. Atomic force microscopy (AFM). The AFM micrographs of abraded mild steel surface as well as after 3 h immersion in 1 M HCl without and with optimum concentration of the investigated inhibitors are shown in Fig. 8. Fig. 8a represents the AFM micrograph of abraded mild steel surface which is relatively smooth with abrading scratches and pits which is resulted due to abrading cleaning of metallic surface from emery papers. The calculated average surface roughness for abraded mild steel surface was 85 nm. The surface of mild steel specimen in the absence of inhibitors was highly corroded, rough and inhomogeneous as shown in Fig. 8b. For the mild steel specimen corroded in free acid solution without inhibitors, the calculated surface roughness is 392 nm. However, in the presence of optimum concentration of the studied inhibitors (Fig. 7c–e) there is significant improvement in the surface smoothness, which is attributed to the adsorption of the inhibitors on mild steel surface and consequently isolation of the metal surface from corrosive medium. The calculated surface roughness decreased to 156, 134, and 108 nm in the presence of DHPC-1, DHPC-2 and DHPC-3, respectively. In other words, the degree of surface smoothness based on AFM analyses is in the order DHPC-3 > DHPC-2 > DHPC-1, which is in accordance with the order of the experimental inhibition efficiencies.

3.4. Theoretical studies

3.4.1. Quantum chemical calculations. The ground state optimized structures of the studied compounds are shown in Fig. 9. The most stable geometries of the three DHPCs correspond to the molecular structures in which the benzenethiolyl group is twisted out of plane and non-coplanar with the chromenopyridine ring. Electron density isosurfaces of the highest occupied molecular orbital (HOMO) and lowest unoccupied molecular orbital (LUMO) of the studied DHPCs are also shown in Fig. 10. The HOMO provides information about the molecular orbitals of the inhibitor that may interact with atomic orbitals of the metal *via* charge donation to the appropriate vacant or partially filled metallic orbitals. The HOMOs of the three compounds comprise both σ- and π-type orbitals and distributed over the entire rings contained in the molecules. In all the three DHPCs, the $-NH_2$ group at the 4-position on the pyridine ring makes little or no contributions to the HOMO. In DHPC-3, the N-atom in the pyridine ring does not contribute to the HOMO. The $-NO_2$ group on the chromene ring of DHPC-1 does not seem to contribute to the HOMO. In all the three compounds, the S-atom of the benzenethiolyl group contributes significantly to the HOMO and shows the tendency of donating charges to the appropriate vacant orbitals of Fe *via* σ-type HOMOs. The LUMO provides information about the molecular orbitals of the inhibitor that may interact with atomic orbitals of the metal by accepting charges from the occupied orbitals of the metallic atom in a retro-donation step. In all the three compounds, the C-atoms in the chromene ring are well involved in the LUMO. The LUMO is also well distributed on the benzenethiolyl group in both DHPC-2 and DHPC-3. However, the benzenethiolyl group does not contribute to the LUMO in DHPC-1. This observation can be attributed to the electron-withdrawing effect of the $-NO_2$ group on the chromene ring of DHPC-1, which may pull the electron density of the benzenethiolyl group towards the chromene ring, and inductively assisted by the highly electronegative S-atom. The N-containing substituent groups on the pyridine ring in DHPC-1 do not contribute to the LUMO, suggesting that these groups cannot participate in backward-donation of charges during the donor–

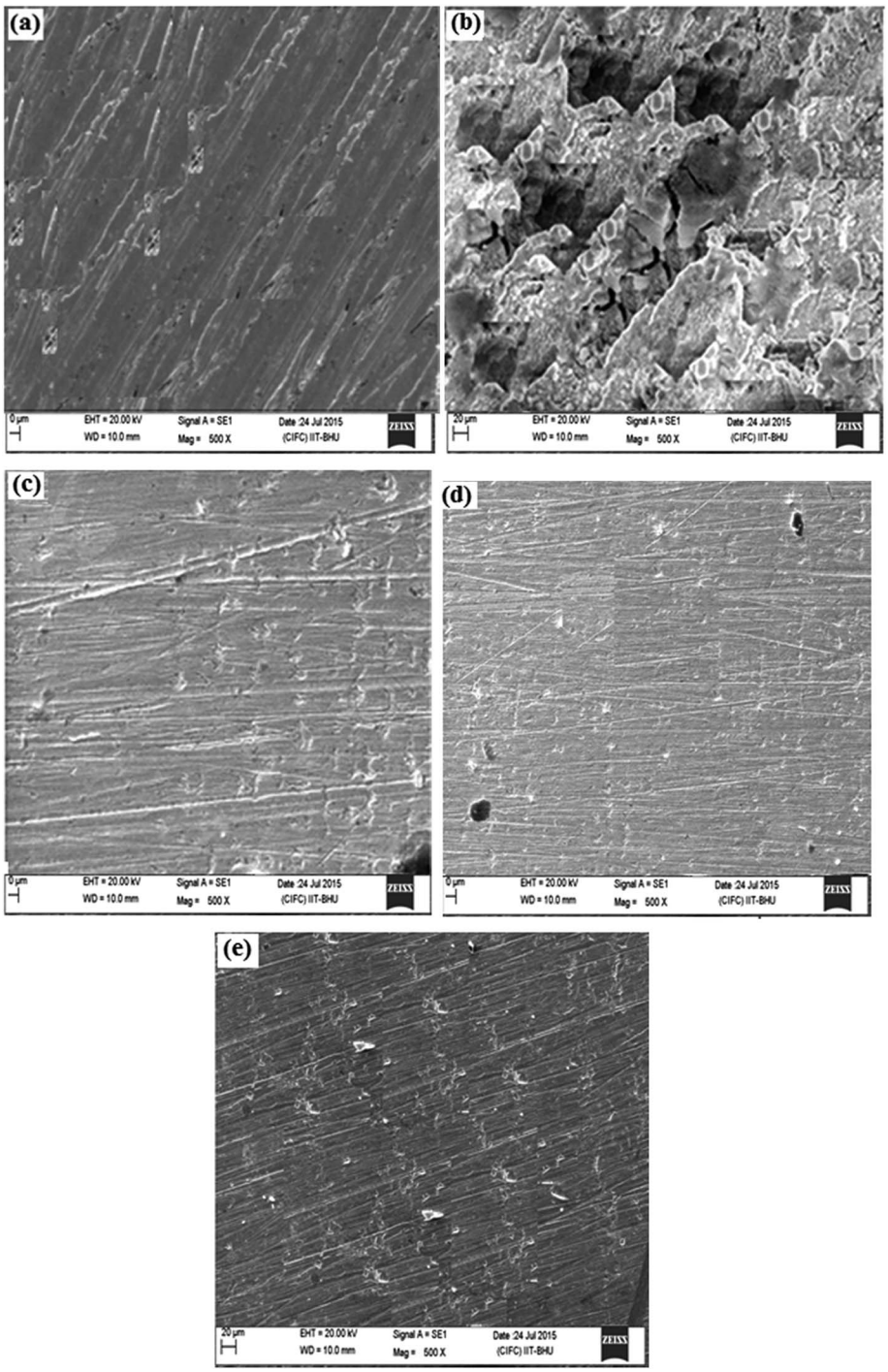

Fig. 7 SEM images of abraded mild steel surface (a), mild steel surface in 1 M HCl in the absence of DHPCs (b), and mild steel surfaces in 1 M HCl containing optimum concentration of DHPC-1 (c), DHPC-2 (d), and DHPC-3 (e).

acceptor interactions between DHPC-1 molecule and Fe. This generalization cannot be made for DHPC-2 and DHPC-3. The values of some relevant quantum chemical parameters for the studied inhibitor molecules are listed in Table 8. The donor–acceptor interactions between an inhibitor molecule and a metal atom are usually correlated with the FMO energies and other related reactivity indices. Generally, the higher the E_{HOMO}, the better the tendency of an inhibitor molecule to donate electrons to the metal, and the lower the E_{LUMO} the better the tendency of an inhibitor molecule to accept electrons from the metal. A low value of the energy gap (ΔE) is also an indication of high reactivity of the inhibitor molecule. For a group of inhibitor molecules with similar molecular architectures, the compound with a higher E_{HOMO}, a lower E_{LUMO} and a lower ΔE usually exhibits higher inhibition efficiency. The results in Table 8 show that the values of E_{HOMO} for the three compounds

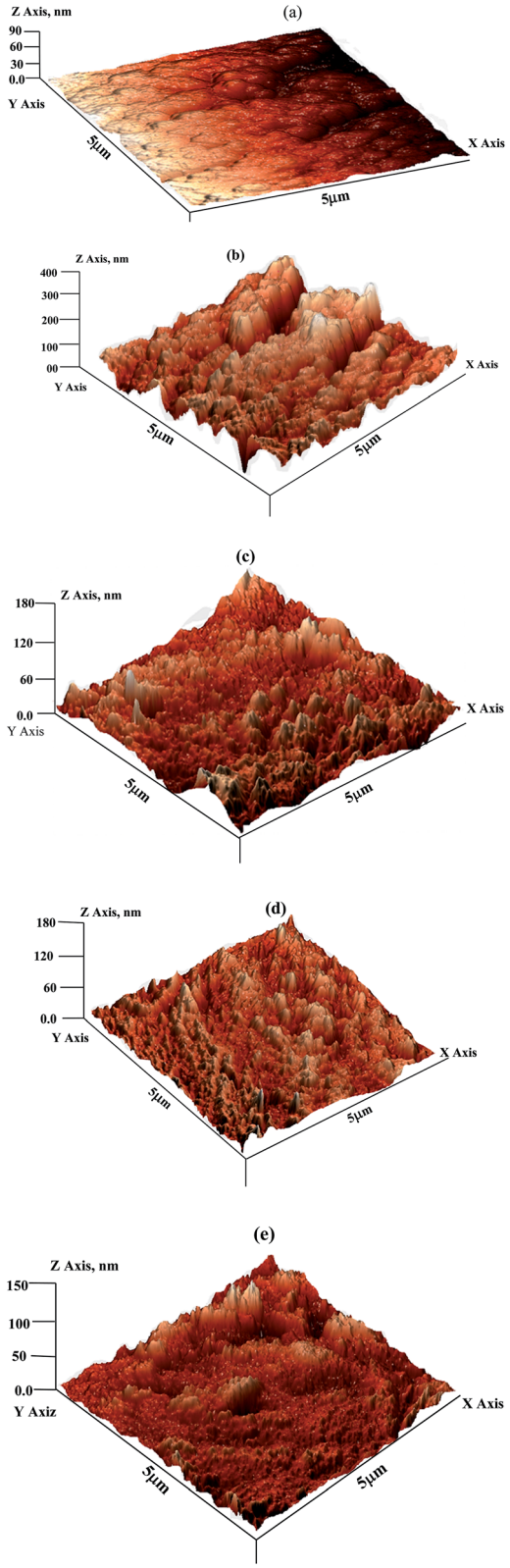

Fig. 8 AFM images of abraded mild steel surface (a), mild steel surface in 1 M HCl in the absence of DHPCs (b), and mild steel surfaces in 1 M HCl containing optimum concentration of DHPC-1 (c), DHPC-2 (d), and DHPC-3 (e).

are in the order: DHPC-3 > DHPC-2 > DHPC-1, which is in agreement with the order of inhibition efficiency of the compounds. This observation suggests that the higher the tendency of a DHPC molecule to donate its least stable electron(s) to the appropriate vacant orbitals of the metal atom, the higher the inhibition efficiency. The values of E_{LUMO} and ΔE listed in Table 8 do not agree with the observed order of inhibition efficiency. Global electronegativity (χ) can be used as a measure of the tendency of a molecule to retain its own electrons during donor/acceptor interactions that lead to corrosion inhibition. It is expected that a low value of χ will inform high inhibition performance. The results in Table 8 reveal that the order of increasing χ values is DHPC-3 < DHCP-2 < DHPC-1, which suggests highest inhibition efficiency for DHPC-3, and the trend is in agreement with the observed inhibition efficiency. The order of dipole moments of the studied inhibitors is DHPC-3 > DHPC-2 > DHPC-1, which is in agreement with the order of inhibition efficiency of the compounds and suggests that higher dipole moment favors higher inhibition potential. The enhanced inhibition performance of a molecule with a high dipole moment has been attributed to increased dipole–dipole interactions between the inhibitor molecule and charged metal surface.[18,47–49] The trend of the values of ΔN for the studied compounds as listed in Table 8 is DHPC-3 > DHPC-2 > DHPC-1. This trend is also in agreement with the order of experimental inhibition efficiency of the compounds. This observation implies that the tendency of a DHPC to inhibit metal corrosion is dependent on its ability to donate a high fraction of electrons to the metal. The values of ΔN in the present study are less than 3.6, which according to Lukovits's study[50] suggest that the inhibition efficiency of DHPCs will increase with increasing electron-donating ability to the metal surface.

The electron density isosurfaces for f^+ and f^- Fukui indices that correspond to nucleophilic and electrophilic attacks respectively are shown in Fig. 11. The graphical representations of f^+ Fukui functions for the studied compounds show that the most susceptible sites of nucleophilic attacks in DHPC-1 are located on the $-NO_2$ substituent on the chromene ring and some neighboring C-atoms in the ring especially those that are adjacent to the electronegative O-atom in the chromene ring. The –C≡N substituent on the pyridine ring is also susceptible to nucleophilic attacks in all the three DHPCs. The prospective sites of nucleophilic attacks in DHPC-2 and DHPC-3 include mainly the C-4 atom of the pyridine ring, the S–C region of the benzenethiolyl group, and the C–C region of the chromene ring adjacent to the benzenthiolyl group. The electron density distributions for the f^- Fukui indices reveal that the sites of electrophilic attacks in the studied DHPCs include essentially the O-atom of the chromene ring, the N-atom of the $-NH_2$ substituent at the 2-position of the pyridine ring, the –N of the –C≡N substituent and the adjacent C-atom in the pyridine ring, the S-atom of the benzenthiolyl group, and the π-electron (C=C) region shared by the fused pyridine and chromene rings. The O-atom of the –OH substituent on chromene ring in DHPC-3 and the adjacent C=C region are also susceptible sites for electrophilic attack.

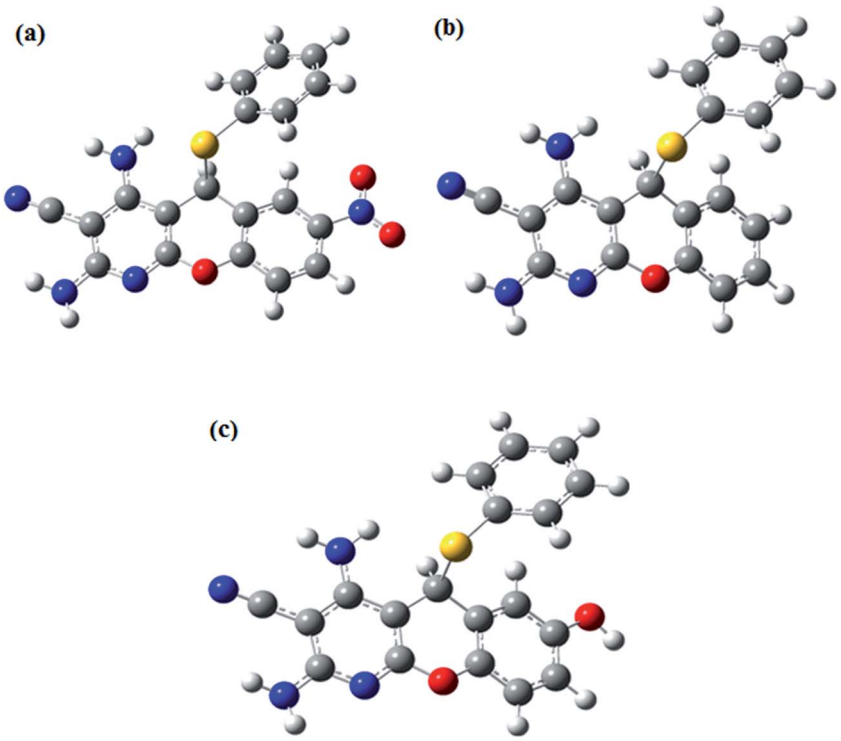

Fig. 9 Optimized molecular structures of (a) DHPC-1, (b) DHPC-2, and (c) DHPC-3.

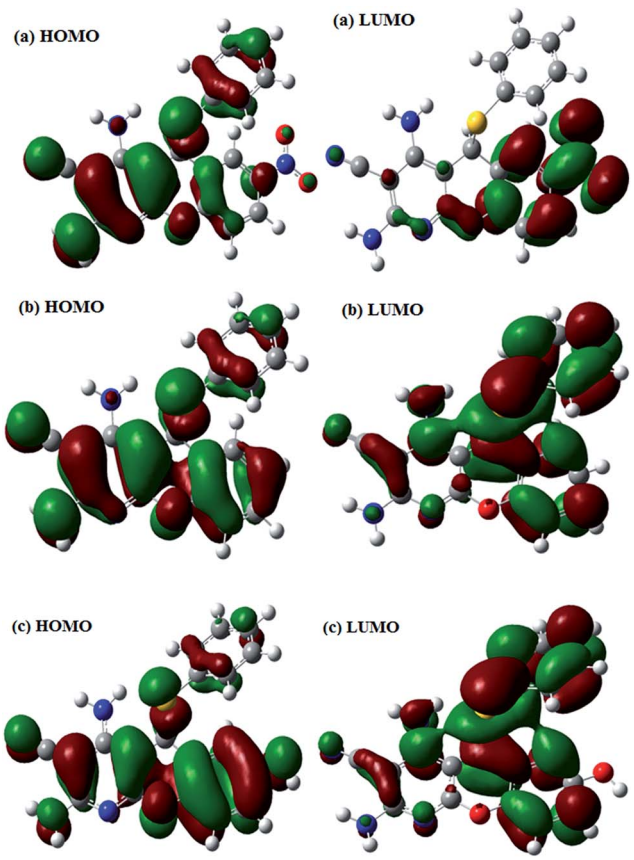

Fig. 10 The frontier molecular orbital (left-hand side: HOMO; and right-hand side: LUMO) of the studied DHPCs (a) DHPC-1 (b) DHPC-2, and (c) DHPC-3.

3.4.2. Molecular dynamics simulations studies. The adsorption behavior of the studied inhibitors on mild steel surface was also investigated using molecular dynamics simulation, which has emerged as a powerful tool to study the adsorption nature of the inhibitor molecule on metallic surface.[51,52] The molecular dynamics simulation has been used to describe the most favorable conformation of the adsorbed inhibitor molecule on the iron surface. Fig. 12 represents the side and top views of the most stable adsorption models of (a) DHPC-1, (b) DHPC-2, and (c) DHPC-3 on Fe (110) surface using quench molecular dynamic and calculated parameters are listed in the Table 9. It is clear from Fig. 12 that all the studied compounds adsorbed on the metallic surface by flat or parallel orientation, which suggests the strong interactions between the inhibitor molecules and Fe (110) surface. The values of interaction energy ($E_{interaction}$) for the studied inhibitors follow the order DHPC-3 > DHPC-2 > DHPC-1, which is agreement with the order of inhibition efficiency of the molecules. The high negative values of interaction energies suggest that the DHPCs spontaneously and strongly adsorb on Fe (110) surface.[18,53] The

Table 8 Some relevant quantum chemical parameters of the studied compounds

Compound	E_{HOMO} (eV)	E_{LUMO} (eV)	ΔE (eV)	χ (eV)	Dipole moment (Debye)	ΔN
DHPC-1	−6.22	−2.42	3.80	4.32	1.75	0.70
DHPC-2	−5.86	−1.15	4.71	3.50	4.31	0.74
DHPC-3	−5.66	−1.14	4.53	3.40	4.85	0.80

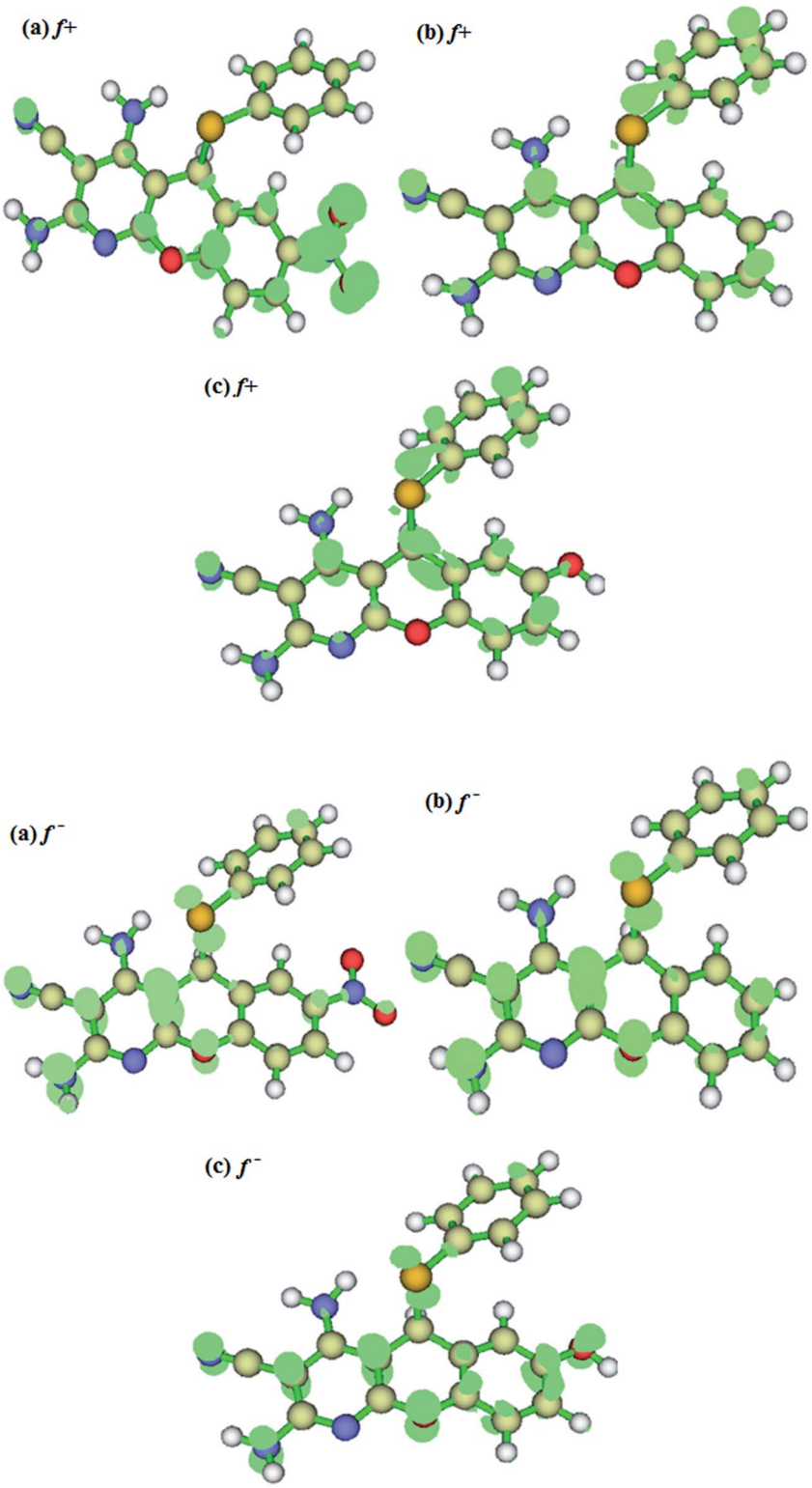

Fig. 11 Fukui indices f^+ and f^- corresponding to the atomics sites for the nucleophilic and electrophilic attacks respectively in (a) DHPC-1, (b) DHPC-2, and (c) DHPC-3 (isosurface value = 0.003).

highest value of $E_{interaction}$ obtained for DHPC-3 among the studied inhibitors implies that it is most strongly adsorbed inhibitor on the metallic surface leading to highest inhibition efficiency. The trend of $E_{interaction}$ obtained for the studied compounds are in good agreement with the order of experimental inhibition efficiency. The values of binding energies ($E_{binding}$), which describe the strength of binding between inhibitor molecules and Fe (110) surface are in the order DHPC-3 > DHPC-2 >

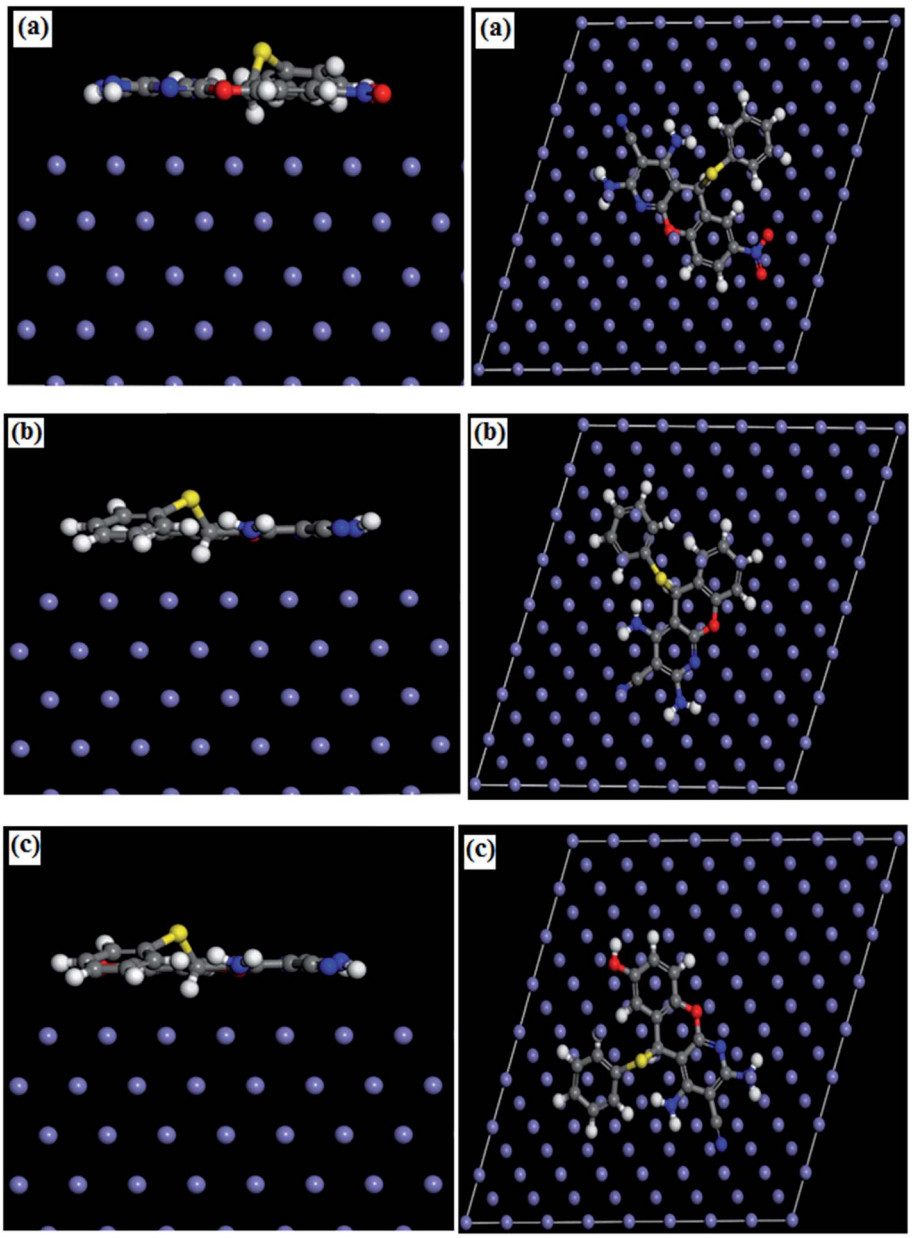

Fig. 12 Side and top views of the most stable adsorption models of (a) DHPC-1, (b) DHPC-2, and (c) DHPC-3 on Fe (110) surface using quench molecular dynamic.

DHPC-1. The values of binding energies ($E_{binding}$) which describes the strength of binding between inhibitor molecules and Fe (110) surface also obeyed the order: DHPC-3 > DHPC-2 > DHPC-1. This finding suggests that DHPC-3 has maximum tendency to adsorb on mild steel surface which resulted in the maximum inhibition efficiency obtained for DHPC-3.[53–55]

Table 9 Interaction energies between the inhibitors and Fe (110) surface (kcal mol^{-1})

Systems	$E_{interaction}$	$E_{binding}$
Fe (110) + DHPC-1	−154.83	154.83
Fe (110) + DHPC-2	−162.77	162.77
Fe (110) + DHPC-3	−188.09	188.09

4. Conclusion

In the present study, combined experimental and theoretical approaches are employed to investigate the inhibition performance of three 2,4-diamino-5-(phenylthio)-5*H*-chromeno[2,3-*b*] pyridine-3-carbonitrile (DHPCs) on mild steel in 1 M HCl solution. The following conclusions were drawn from the results:

1. All the studied DHPCs act as good corrosion inhibitors and their inhibition efficiency increases with increase in concentration, and decrease with increase in temperature.

2. The studied inhibitors significantly elevate the activation energy associated with corrosion reaction and thereby reduce the reaction rate.

3. Polarization study revealed that studied compounds are mixed type inhibitors with predominantly cathodic inhibitive capacity.

4. EIS study revealed that values of charge transfer resistance (R_{ct}) increases in presence of inhibitors due to the adsorption of inhibitors at metal/electrolyte interfaces.

5. The adsorption of DHPCs on mild steel surface obey the Langmuir adsorption isotherm and involves physisorption and chemisorption mechanisms.

6. Quantum chemical calculations provide successful explanations to the observed inhibition efficiencies of the molecules based on the frontier molecular energy parameters.

7. The electrophilic and nucleophilic sites of the inhibitor molecules were identified by Fukui functions.

8. The molecular dynamics simulation study revealed that all the studied inhibitors spontaneously and strongly adsorbed on the Fe (110) surface by flat or parallel orientation and the trend of predicted binding energies agree with experimental inhibition efficiencies.

References

1 Z. El Adnani, M. Mcharfi, M. Sfaira, M. Benzakour, A. T. Benjelloun and M. E. Touhami, *Corros. Sci.*, 2013, **68**, 223–230.
2 A. Zarrouk, B. Hammouti, T. Lakhlifi, M. Traisnel, H. Vezin and F. Bentiss, *Corros. Sci.*, 2015, **90**, 572–584.
3 C. Verma, A. Singh, G. Pallikonda, M. Chakravarty, M. A. Quraishi, I. Bahadur and E. E. Ebenso, *J. Mol. Liq.*, 2015, **209**, 306–319.
4 A. O. Yuce and G. Kardas, *Corros. Sci.*, 2012, **58**, 86–94.
5 M. Abdallah, B. H. Asghar, I. Zaafarany and A. S. Fouda, *Int. J. Electrochem. Sci.*, 2012, **7**, 282–304.
6 C. Verma, P. Singh, I. Bahadur, E. E. Ebenso and M. A. Quraishi, *J. Mol. Liq.*, 2015, **209**, 767–778.
7 L. O. Olasunkanmi, I. B. Obot, M. M. Kabanda and E. E. Ebenso, *J. Phys. Chem. C*, 2015, **119**, 16004–16019.
8 A. M. Fekry and R. R. Mohamed, *Electrochim. Acta*, 2010, **55**, 1933–1939.
9 N. Soltani, M. Behpour, E. E. Oguzie, M. Mahluji and M. A. Ghasemzadeh, *RSC Adv.*, 2015, **5**, 11145–11162.
10 Y. Tang, X. Yang, W. Yang, Y. Chen and R. Wan, *Corros. Sci.*, 2010, **52**, 242–249.
11 E. Rafiee and H. Jafari, *Bioorg. Med. Chem. Lett.*, 2006, **16**, 2463–2466.
12 P. Anastas and N. Eghbali, *Chem. Soc. Rev.*, 2010, **39**, 301–312.
13 M. S. Singh and S. Chowdhury, *RSC Adv.*, 2012, **2**, 4547–4592.
14 R. C. Cioc, E. Ruijter and R. V. A. Orru, *Green Chem.*, 2014, **16**, 2958–2975.
15 J. Martínez, S. Romero-Vega, R. Abeja-Cruz, C. Álvarez-Toledano and R. Miranda, *Int. J. Mol. Sci.*, 2013, **14**, 2903–2915.
16 N. M. Evdokimov, A. S. Kireev, A. A. Yakovenko, M. Y. Antipin, I. V. Magedov and A. Kornienko, *J. Org. Chem.*, 2007, **72**, 3443–3453.
17 C. Verma, E. E. Ebenso, I. Bahadur, I. B. Obot and M. A. Quraishi, *J. Mol. Liq.*, 2015, **212**, 209–218.
18 Y. Sasikumar, A. S. Adekunle, L. O. Olasunkanmi, I. Bahadur, R. Baskar, M. M. Kabanda, I. B. Obot and E. E. Ebenso, *J. Mol. Liq.*, 2015, **211**, 105–118.
19 L. O. Olasunkanmi, M. M. Kabanda and E. E. Ebenso, *Physica E*, 2016, **76**, 109–126.
20 A. D. Becke, *J. Chem. Phys.*, 1993, **98**, 5648–5652.
21 R. G. Parr and W. Yang, *J. Am. Chem. Soc.*, 1984, **106**, 4049–4050.
22 C. Lee, W. Yang and R. G. Parr, *Phys. Rev. B: Condens. Matter Mater. Phys.*, 1988, **37**, 785–789.
23 M. J. Frisch, G. W. Trucks, H. B. Schlegel, G. E. Scuseria, M. A. Robb, J. R. Cheeseman, G. Scalmani, V. Barone, B. Mennucci and G. A. Petersson, *et al.*, *Gaussian 09, Revision D.01*, Gaussian, Inc, Wallingford CT, 2009.
24 B. Gomez, N. V. Likhanova, M. A. Dominguez, R. Martinez-Palou, A. Vela and L. J. Gazquez, *J. Phys. Chem. B*, 2006, **110**, 8928–8934.
25 W. Yang and W. J. Mortier, *J. Am. Chem. Soc.*, 1986, **108**, 5708–5711.
26 T. Lu and F. Chen, *J. Comput. Chem.*, 2012, **33**, 580–592.
27 T. Lu and F. Chen, *J. Mol. Graphics Modell.*, 2012, **38**, 314–323.
28 C. Verma, M. A. Quraishi, L. O. Olasunkanmi and E. E. Ebenso, *RSC Adv.*, 2015, **5**, 85417–85430.
29 A. Ehsani, M. G. Mahjani, R. Moshrefi, H. Mostaanzadeh and J. S. Shayeh, *RSC Adv.*, 2014, **4**, 20031–20037.
30 N. K. Gupta, C. Verma, M. A. Quraishi and A. K. Mukherjee, *J. Mol. Liq.*, 2016, **215**, 47–57.
31 N. Weder, R. A. Alberto and R. Koitz, *J. Phys. Chem. C*, 2016, **120**, 1770–1777.
32 S. Ghareba and S. Omanovic, *Corros. Sci.*, 2010, **52**, 2104–2113.
33 M. A. Amin and M. M. Ibrahim, *Corros. Sci.*, 2011, **53**, 873–885.
34 S. Issaadi, T. Douadi, A. Zouaoui, S. Chafaa, M. A. Khan and G. Bouet, *Corros. Sci.*, 2011, **53**, 1484–1488.
35 M. A. Amin, M. A. Ahmed, H. A. Arida, T. Arslan, M. Saraçoglu and F. Kandemirli, *Corros. Sci.*, 2011, **53**, 540–548.
36 F. Bentiss, M. Lebrini and M. Lagrenee, *Corros. Sci.*, 2005, **47**, 2915–2931.
37 R. Yıldız, T. Dogan and I. Dehri, *Corros. Sci.*, 2014, **85**, 215–221.
38 R. Solmaz, *Corros. Sci.*, 2014, **81**, 75–84.
39 C. Christodoulou, C. I. Goodier, S. A. Austin, J. Webb and G. Glass, *Corros. Sci.*, 2012, **62**, 176–183.
40 R. A. Bustamante, G. N. Silve, M. A. Quijano, H. H. Hernandez, M. R. Romo, A. Cuan and M. P. Pardave, *Electrochim. Acta*, 2009, **54**, 5393–5399.
41 D. K. Yadav and M. A. Quraishi, *Ind. Eng. Chem. Res.*, 2012, **51**, 14966–14979.

42 M. Yadav, S. Kumar, N. Tiwari, I. Bahadur and E. E. Ebenso, *J. Mol. Liq.*, 2015, **212**, 151–167.
43 P. Roy, P. Karfa, U. Adhikar and D. Sukul, *Corros. Sci.*, 2014, **88**, 246–253.
44 D. Gopi, P. Karthikeyana, L. Kavithac and M. Surendiran, *Appl. Surf. Sci.*, 2015, **357**, 122–130.
45 C. Verma, M. A. Quraishi and A. Singh, *J. Taiwan Inst. Chem. Eng.*, 2015, **49**, 229–239.
46 E. E. Ebenso, M. M. Kabanda, L. C. Murulana, A. K. Singh and S. K. Shukla, *Ind. Eng. Chem. Res.*, 2012, **51**, 12940–12958.
47 M. S. Nooshabadi, M. Behpour, F. S. Razavi, M. Hamadanian and V. Nejadshafiee, *RSC Adv.*, 2015, **5**, 23357–23366.
48 E. E. Oguzie, C. K. Enenebeaku, C. O. Akalezi, S. C. Okoro, A. A. Ayuk and E. N. Ejike, *J. Colloid Interface Sci.*, 2010, **349**, 283–292.
49 S. T. Arab, *Mater. Res. Bull.*, 2008, **43**, 510–521.
50 I. Lukovits, E. Kalman and F. Zucchi, *Corrosion*, 2001, **57**, 3–8.
51 S. K. Saha, A. Dutta, P. Ghosh, D. Sukul and P. Banerjee, *Phys. Chem. Chem. Phys.*, 2015, **17**, 5679–5690.
52 F. Zhang, Y. Tang, Z. Cao, W. Jing, Z. Wua and Y. Chen, *Corros. Sci.*, 2012, **61**, 1–9.
53 K. F. Khaled and A. El-Maghraby, *Arabian J. Chem.*, 2014, **7**, 319–326.
54 K. F. Khaled, *Corros. Sci.*, 2010, **52**, 3225–3234.
55 C. Verma, L. O. Olasunkanmi, I. B. Obot, E. E. Ebenso and M. A. Quraishi, *RSC Adv.*, 2016, **6**, 15639–15654.